

Ultra-Dense Networks: A New Look at the Proportional Fair Scheduler

Ming Ding[‡], David López Pérez[†], Amir H. Jafari*, Guoqiang Mao^{‡‡}, Zihuai Lin[¶]

[‡]Data61, Australia, [†]Nokia Bell Labs, Ireland

^{‡‡}School of Computing and Communication, University of Technology Sydney, Australia

*Dept. of Electronic & Electrical Engineering, University of Sheffield, UK

[¶]The University of Sydney, Australia

Abstract—In this paper, we theoretically study the proportional fair (PF) scheduler in the context of ultra-dense networks (UDNs). Analytical results are obtained for the coverage probability and the area spectral efficiency (ASE) performance of dense small cell networks (SCNs) with the PF scheduler employed at base stations (BSs). The key point of our analysis is that the typical user is no longer a random user as assumed in most studies in the literature. Instead, a user with the maximum PF metric is chosen by its serving BS as the typical user. By comparing the previous results of the round-robin (RR) scheduler with our new results of the PF scheduler, we quantify the loss of the multi-user diversity of the PF scheduler with the network densification, which casts a new look at the role of the PF scheduler in UDNs. Our conclusion is that the RR scheduler should be used in UDNs to simplify the radio resource management (RRM).

I. INTRODUCTION

Network densification is envisioned to be the key solution to meet users' traffic demands in the 5th-generation (5G) networks [1]. Indeed, the orthogonal deployment¹ of dense small cell networks (SCNs) within the existing macrocell networks [2] has been the workhorse for capacity enhancement in the 4th-generation (4G), developed by the 3rd Generation Partnership Project (3GPP), and this approach to capacity enhancement will continue in 5G with the adoption of ultra-dense networks (UDNs) [1, 3]. In this paper, we focus on the analysis of such orthogonal deployment of UDNs.

Despite of its benefits, the SCN densification also opens up new research questions. In particular, scheduling has been conceived as an effective technique used at base stations (BSs) to efficiently use the available spectrum and improve the overall system throughput. In most cases, a proportional fair (PF) scheduler [4] serves as an appealing technique that offers a good trade-off between maximizing overall throughput and improving fairness among user equipments (UEs) with diverse channel conditions. However, the gains of the PF scheduler may be limited in UDNs, mostly because the number of UEs per active BS is considerably reduced. This gives rise to the question of *whether the PF scheduling is as efficient for UDNs as it is for sparse networks*, or whether it can be substituted by other ones of lower complexity, such as a round-robin (RR)

one that semi-randomly selects UEs to serve. In this paper, we answer this fundamental question by theoretical analyses.

To the best of our knowledge, there has been no prior work on the theoretical study of the PF scheduler in the context of UDNs, the density of which could be as large as tens of thousands of BSs per km² [1]. Generally speaking, the existing work on PF schedulers does not scale well with the network densification. In more detail, the studies in the literature can be classified into 3 categories: (i) analysis of a scenario with merely one BS [4, 5], (ii) analysis of a scenario with a limited number of BSs [6, 7], which quickly becomes computationally infeasible for UDNs, and (iii) system-level simulations for large-scale networks [8], which lacks analytical rigor.

Compared with the existing work, the main contributions of this paper are:

- For the first time, we use stochastic geometry [9] to derive the analytical results of the coverage probability and the area spectral efficiency (ASE) performance for UDNs with the PF schedulers used at BSs. The key point of our analysis is that the typical user is no longer a random user as assumed in most studies of stochastic geometry [9].
- By comparing the previous results of the RR scheduler and our new results of the PF scheduler, we quantify the loss of the multi-user diversity of the PF scheduler with the network densification, which leads to the conclusion that the RR scheduler should be used in UDNs to simplify the radio resource management (RRM).

II. NETWORK SCENARIO AND SYSTEM MODEL

In this section, we present the network scenario, the wireless system model and the PF scheduler considered in this paper.

A. Network Scenario

For a certain time-frequency resource block, we consider a downlink (DL) cellular network with BSs deployed on a plane according to a homogeneous Poisson point process (HPPP) Φ with a density of λ BSs/km². Active UEs are also Poisson distributed in the considered DL network with a density of ρ UEs/km². Here, we only consider active UEs in the network because non-active UEs do not trigger data transmission. As shown in [1], a typical density of the active UEs in 5G is around 300 UEs/km².

¹The orthogonal deployment means that small cells and macrocells operate on different frequency spectrum, i.e., Small Cell Scenario #2a [2]).

In practice, a BS will enter an idle mode if there is no UE connected to it, which reduces the interference to neighboring UEs as well as the energy consumption of the network. The set of active BSs should be determined by a user association strategy (UAS). In this paper, we assume a practical UAS as in [10], where each UE is connected to the BS having the maximum average received signal strength, which will be formally presented in Subsection II-B.

Note that such BS idle mode operation is not trivial, which even changes the capacity scaling law [11]. Since UEs are randomly and uniformly distributed in the network, we assume that the active BSs also follow an HPPP distribution $\tilde{\Phi}$ [12], the density of which is denoted by $\tilde{\lambda}$ BSs/km². Note that $\tilde{\lambda} \leq \lambda$ and $\tilde{\lambda} \leq \rho$, since one UE is served by at most one BS.

From [12, 13], $\tilde{\lambda}$ is given by

$$\tilde{\lambda} = \lambda \left[1 - \frac{1}{\left(1 + \frac{\rho}{q\lambda}\right)^q} \right], \quad (1)$$

where according to [13], q depends on the path loss model, which will be presented in Subsection II-B.

According to [12], the per-BS coverage area size X can be approximately characterized by a Gamma distribution and the probability density function (PDF) of X can be expressed as

$$f_X(x) = (q\lambda)^q x^{q-1} \frac{\exp(-q\lambda x)}{\Gamma(q)}, \quad (2)$$

where $\Gamma(\cdot)$ is the Gamma function [14]. The UE number per BS is denoted by a random variable (RV) K , and the probability mass function (PMF) of K can be calculated as

$$\begin{aligned} f_K(k) &= \Pr[K = k] \\ &\stackrel{(a)}{=} \int_0^{+\infty} \frac{(\rho x)^k}{k!} \exp(-\rho x) f_X(x) dx \\ &\stackrel{(b)}{=} \frac{\Gamma(k+q)}{\Gamma(k+1)\Gamma(q)} \left(\frac{\rho}{\rho + q\lambda} \right)^k \left(\frac{q\lambda}{\rho + q\lambda} \right)^q, \end{aligned} \quad (3)$$

where (a) is due to the HPPP distribution of UEs and (b) is obtained from (2). It can be seen from (3) that K follows a Negative Binomial distribution [14], i.e., $K \sim \text{NB}\left(q, \frac{\rho}{\rho + q\lambda}\right)$.

As discussed in Subsection II-A, we assume that a BS with $K = 0$ is not active. Thus, we focus on the active BSs and denote the UE number per active BS by a positive RV \tilde{K} . Considering (3), we can conclude that \tilde{K} follows a truncated Negative Binomial distribution, the PMF of which is denoted by $f_{\tilde{K}}(\tilde{k})$, $\tilde{k} \in \{1, 2, \dots, +\infty\}$ and can be written as

$$f_{\tilde{K}}(\tilde{k}) = \Pr[\tilde{K} = \tilde{k}] = \frac{f_K(\tilde{k})}{1 - f_K(0)}. \quad (4)$$

Furthermore, the cumulative mass function (CMF) of \tilde{K} can be written as

$$F_{\tilde{K}}(\tilde{k}) = \sum_{t=1}^{\tilde{k}} f_{\tilde{K}}(t). \quad (5)$$

B. Wireless System Model

Following [10], we adopt a general path loss model, where the path loss $\zeta(r)$ is a multi-piece function of r written as

$$\zeta(r) = \begin{cases} \zeta_1(r), & \text{when } 0 \leq r \leq d_1 \\ \zeta_2(r), & \text{when } d_1 < r \leq d_2 \\ \vdots & \vdots \\ \zeta_N(r), & \text{when } r > d_{N-1} \end{cases}, \quad (6)$$

where each piece $\zeta_n(r)$, $n \in \{1, 2, \dots, N\}$ is modeled as

$$\zeta_n(r) = \begin{cases} \zeta_n^L(r) = A_n^L r^{-\alpha_n^L}, & \text{LoS Prob.: } \Pr_n^L(r) \\ \zeta_n^{NL}(r) = A_n^{NL} r^{-\alpha_n^{NL}}, & \text{NLoS Prob.: } 1 - \Pr_n^L(r) \end{cases}, \quad (7)$$

where

- $\zeta_n^L(r)$ and $\zeta_n^{NL}(r)$, $n \in \{1, 2, \dots, N\}$ are the n -th piece path loss functions for the LoS transmission and the NLoS transmission, respectively,
- A_n^L and A_n^{NL} are the path losses at a reference distance $r = 1$ for the LoS and the NLoS cases, respectively,
- α_n^L and α_n^{NL} are the path loss exponents for the LoS and the NLoS cases, respectively.

Moreover, $\Pr_n^L(r)$ is the n -th piece LoS probability function that a transmitter and a receiver separated by a distance r has a LoS path, which is assumed to be a *monotonically decreasing function* with regard to r [15, 16].

As a special case to show our analytical results, we consider the two-piece path loss and the exponential LoS probability functions defined by the 3GPP [15]. Specifically, we have $N = 2$, $\zeta_1^L(w) = \zeta_2^L(w) = A^L w^{-\alpha^L}$, $\zeta_1^{NL}(w) = \zeta_2^{NL}(w) = A^{NL} w^{-\alpha^{NL}}$, $\Pr_1^L(w) = 1 - 5 \exp(-R_1/w)$, and $\Pr_2^L(w) = 5 \exp(-w/R_2)$, where $R_1 = 156$ m, $R_2 = 30$ m, and $d_1 = \frac{R_1}{\ln 10} = 67.75$ m [15]. For clarity, this case is referred to as **the 3GPP Case** hereafter.

As discussed in Subsection II-A, we assume that each UE is connected to the BS having the maximum average received signal strength, which is equivalent to the BS with the largest $\zeta(r)$. Finally, we assume that each BS/UE is equipped with an isotropic antenna, and that the multi-path fading between a BS and a UE is modeled as independently identical distributed (i.i.d.) Rayleigh fading [10]. In order to make the 3GPP Case even more practical, we will further consider distance-dependent Rician fading [16] in our simulations to show their minor impact on our conclusions. More specifically, we adopt the practical Rician fading defined in the 3GPP [16], where the K factor in dB unit (the ratio between the power in the direct path and the power in the other scattered paths) is modeled as $K[\text{dB}] = 13 - 0.03r$, where r is the distance in meter.

C. The PF Scheduler

The original operation of the PF scheduler is as follows [4],

- First, the average throughput of each UE is tracked by an exponential moving average at the BS.
- Second, each UE frequently feeds back its channel state information (CSI) to its serving BS, so that such BS can calculate the ratio of the instantaneous achievable rate to

the average throughput for each user, which is defined as a PF metric for UE selection.

- Finally, the UE with the maximum PF metric will be selected for DL transmission, which is formulated as

$$u^* = \arg \max_{u \in \{1, 2, \dots, \tilde{k}\}} \left\{ \frac{\tilde{R}_u}{\bar{R}_u} \right\}, \quad (8)$$

where u , u^* , \tilde{R}_u and \bar{R}_u denote the UE index, the selected UE index, the instantaneous achievable rate of UE u and the average throughput of UE u , respectively. Note that the distribution of \tilde{k} has been discussed in (4).

From a network performance analysis point of view, it is very difficult, if not impossible, to analyze the original PF scheduler given by (8). This is because that the objective of a performance analysis is usually to derive the average user throughput \bar{R}_u or aggregate inter-cell interference, but in this case it is part of the PF metric, i.e., $\frac{\tilde{R}_u}{\bar{R}_u}$, and it should be known and plugged into the UE selection criterion of (8) before the performance analysis of \bar{R}_u is carried out. A widely adopted approach to tackle this dilemma is to use alternative measures of CSI in a PF metric, instead of \tilde{R}_u and \bar{R}_u [4–7].

Here, we follow the framework developed in [4], where the authors proposed to use the ratio of the instantaneous signal-to-noise ratio (SNR) to the average SNR as a PF metric instead of the original one. More specifically, the UE selection criterion of the PF scheduler proposed in [4] is given by

$$u^* = \arg \max_{u \in \{1, 2, \dots, \tilde{k}\}} \left\{ \frac{\tilde{Z}_u}{\bar{Z}_u} \right\}, \quad (9)$$

where \tilde{Z}_u and \bar{Z}_u denote the instantaneous SNR of UE u and the average SNR of UE u , respectively. **Although this criterion of (9) is not exactly the same as that of (8), it captures the important characteristics of the PF scheduler:** (i) allowing preference to UEs with relatively good instantaneous channels with respect to their average ones since \tilde{R}_u is a strictly monotonically increasing function of \tilde{Z}_u , and (ii) allocating the same portion of resource to each UE in the long term to enforce fairness, because the chance of $\tilde{Z}_u \geq \bar{Z}_u$ is almost the same for all UEs. Since the accuracy and the practicality of (9) have been well established in [4], we will focus on studying the PF scheduler characterized by (9).

III. MAIN RESULTS

In this section, we study the coverage probability and the ASE performance of a typical UE located at the origin o .

A. The Coverage Probability

First, we investigate the coverage probability that the typical UE's signal-to-interference-plus-noise ratio (SINR) is above a designated threshold γ :

$$p^{\text{cov}}(\lambda, \gamma) = \Pr[\text{SINR} > \gamma], \quad (19)$$

where the typical UE's SINR is computed by

$$\text{SINR} = \frac{P\zeta(r)y(\tilde{k})}{I_{\text{agg}} + P_N}, \quad (20)$$

where $y(\tilde{k})$ is the channel gain on condition of the UE number \tilde{k} , P and P_N are the BS transmission power and the additive white Gaussian noise (AWGN) power at each UE, respectively, and I_{agg} is the cumulative interference given by

$$I_{\text{agg}} = \sum_{i: b_i \in \tilde{\Phi} \setminus b_o} P\beta_i g_i, \quad (21)$$

where b_o is the BS serving the typical UE, and b_i , β_i and g_i are the i -th interfering BS, the path loss from b_i to the typical UE and the multi-path fading channel gain associated with b_i (exponentially distributed), respectively. Note that in (21), only the BSs in $\tilde{\Phi} \setminus b_o$ inject effective interference into the network, where $\tilde{\Phi}$ denotes the set of the active BSs.

It is very important to note that the distribution of $y(\tilde{k})$ should be derived according to (9). More specifically, based on the variable definition in (20), we can reformulate (9) as

$$u^* = \arg \max_{u \in \{1, 2, \dots, \tilde{k}\}} \left\{ \frac{\frac{P\zeta(r)h_u}{P_N}}{\frac{P\zeta(r) \times 1}{P_N}} \right\} = \arg \max_{u \in \{1, 2, \dots, \tilde{k}\}} \{h_u\}, \quad (22)$$

where h_u is an i.i.d. RV with a unit-mean exponential distribution due to our consideration of Rayleigh fading mentioned in Subsection II-B. Thus, $y(\tilde{k})$ can be modeled as the maximum RV of \tilde{k} i.i.d. exponential RVs. The complementary cumulative distribution function (CCDF) of $y(\tilde{k})$ is [17]

$$\bar{F}_{Y(\tilde{k})}(y) = \Pr[Y(\tilde{k}) > y] = 1 - (1 - \exp(-y))^{\tilde{k}}. \quad (23)$$

It is easy to see that $\Pr[Y(\tilde{k}) > y]$ increases as \tilde{k} grows, which in turn improves the typical UE's channel gain. Note that for the RR scheduler, the typical UE is randomly selected in the BS. Consequently, we have that $\tilde{k} = 1$ in (23) and the analytical results for RR have been derived in [13].

Based on the path loss model in (6) and the PF scheduler model in (9), we present our result of $p^{\text{cov}}(\lambda, \gamma)$ in Theorem 1.

Digging into Theorem 1 and considering the truncated Negative Binomial distribution of the UE number per active BS, \tilde{K} , we present our results on $\mathbb{E}_{[\tilde{k}]} \left\{ \Pr \left[\frac{P\zeta_n^{\text{L}}(r)y(\tilde{k})}{I_{\text{agg}} + P_N} > \gamma \right] \right\}$

and $\mathbb{E}_{[\tilde{k}]} \left\{ \Pr \left[\frac{P\zeta_n^{\text{NL}}(r)y(\tilde{k})}{I_{\text{agg}} + P_N} > \gamma \right] \right\}$ in Theorem 2.

Plugging Theorem 2 into Theorem 1, yields our theoretical results on $p^{\text{cov}}(\lambda, \gamma)$. From Theorems 1 and 2, we can draw an important and intuitive conclusion in Lemma 3.

Lemma 3. *The $p^{\text{cov}}(\lambda, \gamma)$ of the PF scheduler converges to that of the RR scheduler as $\lambda \rightarrow +\infty$.*

Proof: See Appendix C. ■

Although we have obtained the closed-form expressions of $p^{\text{cov}}(\lambda, \gamma)$ for the PF scheduler in Theorems 1 and 2, it is im-

Theorem 1. Considering the path loss model in (6) and the PF scheduler model in (9), we can derive $p^{\text{cov}}(\lambda, \gamma)$ as

$$p^{\text{cov}}(\lambda, \gamma) = \sum_{n=1}^N (T_n^{\text{L}} + T_n^{\text{NL}}), \quad (10)$$

where $T_n^{\text{L}} = \int_{d_{n-1}}^{d_n} \mathbb{E}_{[\tilde{k}]} \left\{ \Pr \left[\frac{P\zeta_n^{\text{L}}(r)y(\tilde{k})}{I_{\text{agg}} + P_{\text{N}}} > \gamma \right] \right\} f_{R,n}^{\text{L}}(r) dr$, $T_n^{\text{NL}} = \int_{d_{n-1}}^{d_n} \mathbb{E}_{[\tilde{k}]} \left\{ \Pr \left[\frac{P\zeta_n^{\text{NL}}(r)y(\tilde{k})}{I_{\text{agg}} + P_{\text{N}}} > \gamma \right] \right\} (r) dr$, and d_0 and d_N are defined as 0 and $+\infty$, respectively. Moreover, $f_{R,n}^{\text{L}}(r)$ and $f_{R,n}^{\text{NL}}(r)$ ($d_{n-1} < r \leq d_n$), are represented by

$$f_{R,n}^{\text{L}}(r) = \exp \left(- \int_0^{r_1} (1 - \Pr^{\text{L}}(u)) 2\pi u \lambda du \right) \exp \left(- \int_0^r \Pr^{\text{L}}(u) 2\pi u \lambda du \right) \Pr_n^{\text{L}}(r) 2\pi r \lambda, \quad (11)$$

and

$$f_{R,n}^{\text{NL}}(r) = \exp \left(- \int_0^{r_2} \Pr^{\text{L}}(u) 2\pi u \lambda du \right) \exp \left(- \int_0^r (1 - \Pr^{\text{L}}(u)) 2\pi u \lambda du \right) (1 - \Pr_n^{\text{L}}(r)) 2\pi r \lambda, \quad (12)$$

where $r_1 = \arg \left\{ \zeta_n^{\text{NL}}(r_1) = \zeta_n^{\text{L}}(r) \right\}$ and $r_2 = \arg \left\{ \zeta_n^{\text{L}}(r_2) = \zeta_n^{\text{NL}}(r) \right\}$.

Proof: See Appendix A. ■

Theorem 2. Considering the truncated Negative Binomial distribution of the UE number per active BS, \tilde{K} , characterized in (4), we can derive $\mathbb{E}_{[\tilde{k}]} \left\{ \Pr \left[\frac{P\zeta_n^{\text{L}}(r)y(\tilde{k})}{I_{\text{agg}} + P_{\text{N}}} > \gamma \right] \right\}$, which will be used in Theorem 1 as

$$\mathbb{E}_{[\tilde{k}]} \left\{ \Pr \left[\frac{P\zeta_n^{\text{L}}(r)y(\tilde{k})}{I_{\text{agg}} + P_{\text{N}}} > \gamma \right] \right\} = \sum_{\tilde{k}=1}^{\tilde{K}^{\text{max}}} \left[1 - \sum_{t=0}^{\tilde{k}} \binom{\tilde{k}}{t} (-\delta_n^{\text{L}}(r))^t \mathcal{L}_{I_{\text{agg}}}^{\text{L}} \left(\frac{t\gamma}{P\zeta_n^{\text{L}}(r)} \right) \right] f_{\tilde{K}}(\tilde{k}), \quad (13)$$

where \tilde{K}^{max} is a large enough integer that makes $F_{\tilde{K}}(\tilde{K}^{\text{max}})$ in (5) close to one with a gap of a small value ϵ so that the expectation value in (13) can be accurately evaluated over \tilde{k} , $f_{\tilde{K}}(\tilde{k})$ is obtained from (4), $\delta_n^{\text{L}}(r)$ is expressed by

$$\delta_n^{\text{L}}(r) = \exp \left(- \frac{\gamma P_{\text{N}}}{P\zeta_n^{\text{L}}(r)} \right), \quad (14)$$

and $\mathcal{L}_{I_{\text{agg}}}^{\text{L}}(s)$ is the Laplace transform of I_{agg} for LoS signal transmission evaluated at s , which can be further written as

$$\mathcal{L}_{I_{\text{agg}}}^{\text{L}}(s) = \exp \left(- 2\pi \tilde{\lambda} \int_r^{+\infty} \frac{\Pr^{\text{L}}(u) u}{1 + (sP\zeta^{\text{L}}(u))^{-1}} du \right) \exp \left(- 2\pi \tilde{\lambda} \int_{r_1}^{+\infty} \frac{[1 - \Pr^{\text{L}}(u)] u}{1 + (sP\zeta^{\text{NL}}(u))^{-1}} du \right). \quad (15)$$

In a similar way, $\mathbb{E}_{[\tilde{k}]} \left\{ \Pr \left[\frac{P\zeta_n^{\text{NL}}(r)y(\tilde{k})}{I_{\text{agg}} + P_{\text{N}}} > \gamma \right] \right\}$ is computed by

$$\mathbb{E}_{[\tilde{k}]} \left\{ \Pr \left[\frac{P\zeta_n^{\text{NL}}(r)y(\tilde{k})}{I_{\text{agg}} + P_{\text{N}}} > \gamma \right] \right\} = \sum_{\tilde{k}=1}^{\tilde{K}^{\text{max}}} \left[1 - \sum_{t=0}^{\tilde{k}} \binom{\tilde{k}}{t} (-\delta_n^{\text{NL}}(r))^t \mathcal{L}_{I_{\text{agg}}}^{\text{NL}} \left(\frac{t\gamma}{P\zeta_n^{\text{NL}}(r)} \right) \right] f_{\tilde{K}}(\tilde{k}), \quad (16)$$

where $\delta_n^{\text{NL}}(r)$ is expressed by

$$\delta_n^{\text{NL}}(r) = \exp \left(- \frac{\gamma P_{\text{N}}}{P\zeta_n^{\text{NL}}(r)} \right), \quad (17)$$

and $\mathcal{L}_{I_{\text{agg}}}^{\text{NL}}(s)$ is the Laplace transform of I_{agg} for NLoS signal transmission evaluated at s , which can be further written as

$$\mathcal{L}_{I_{\text{agg}}}^{\text{NL}}(s) = \exp \left(- 2\pi \tilde{\lambda} \int_{r_2}^{+\infty} \frac{\Pr^{\text{L}}(u) u}{1 + (sP\zeta^{\text{L}}(u))^{-1}} du \right) \exp \left(- 2\pi \tilde{\lambda} \int_r^{+\infty} \frac{[1 - \Pr^{\text{L}}(u)] u}{1 + (sP\zeta^{\text{NL}}(u))^{-1}} du \right). \quad (18)$$

Proof: See Appendix B. ■

Theorem 4. $\mathbb{E}_{[\tilde{k}]} \left\{ \Pr \left[\frac{P\zeta_n^L(r)y(\tilde{k})}{I_{\text{agg}} + P_N} > \gamma \right] \right\}$ and $\mathbb{E}_{[\tilde{k}]} \left\{ \Pr \left[\frac{P\zeta_n^{\text{NL}}(r)y(\tilde{k})}{I_{\text{agg}} + P_N} > \gamma \right] \right\}$ can be respectively upper bounded by

$$\mathbb{E}_{[\tilde{k}]} \left\{ \Pr \left[\frac{P\zeta_n^L(r)y(\tilde{k})}{I_{\text{agg}} + P_N} > \gamma \right] \right\} \leq \sum_{\tilde{k}=1}^{\tilde{K}^{\text{max}}} \left\{ 1 - \left[1 - \delta_n^L(r) \mathcal{L}_{I_{\text{agg}}}^L \left(\frac{\gamma}{P\zeta_n^L(r)} \right) \right]^{\tilde{k}} \right\} f_{\tilde{K}}(\tilde{k}), \quad (24)$$

and

$$\mathbb{E}_{[\tilde{k}]} \left\{ \Pr \left[\frac{P\zeta_n^{\text{NL}}(r)y(\tilde{k})}{I_{\text{agg}} + P_N} > \gamma \right] \right\} \leq \sum_{\tilde{k}=1}^{\tilde{K}^{\text{max}}} \left\{ 1 - \left[1 - \delta_n^{\text{NL}}(r) \mathcal{L}_{I_{\text{agg}}}^{\text{NL}} \left(\frac{\gamma}{P\zeta_n^{\text{NL}}(r)} \right) \right]^{\tilde{k}} \right\} f_{\tilde{K}}(\tilde{k}). \quad (25)$$

Proof: See Appendix D. ■

portant to note that Theorem 2 is computationally intensive for the case of sparse networks, where the maximum UE number per active BS \tilde{K}^{max} could be very large, leading to complex computations for $\mathcal{L}_{I_{\text{agg}}}^L \left(\frac{t\gamma}{P\zeta_n^L(r)} \right)$ and $\mathcal{L}_{I_{\text{agg}}}^{\text{NL}} \left(\frac{t\gamma}{P\zeta_n^{\text{NL}}(r)} \right)$, $t \in \{0, 1, \dots, \tilde{K}^{\text{max}}\}$ in (15) and (18), respectively. For example, when the UE density is $\rho = 300$ UEs/km² and the BS density is $\lambda = 10$ BSs/km², \tilde{K}^{max} should be as large as 102 to make $F_{\tilde{K}}(\tilde{K}^{\text{max}})$ sufficiently close to one with a gap smaller than $\epsilon = 0.001$. As a result, we need to calculate the integrals in (15) and (18) at least 102 times for every possible value of r . The good news is that Theorem 2 is very efficient for 5G UDNs, where \tilde{K}^{max} is expected to be less than 10 [1]. In the next subsection, we derive alternative and more efficient expressions for sparse networks.

B. A Low-Complexity Upper-Bound of $p^{\text{cov}}(\lambda, \gamma)$

We present upper bounds of $\mathbb{E}_{[\tilde{k}]} \left\{ \Pr \left[\frac{P\zeta_n^L(r)y(\tilde{k})}{I_{\text{agg}} + P_N} > \gamma \right] \right\}$ and $\mathbb{E}_{[\tilde{k}]} \left\{ \Pr \left[\frac{P\zeta_n^{\text{NL}}(r)y(\tilde{k})}{I_{\text{agg}} + P_N} > \gamma \right] \right\}$ in Theorem 4.

The proposed upper bounds in Theorem 4 require to calculate the integrals in (15) and (18) *only once* for every possible value of r , which makes the analysis of sparse networks very efficient. Consequently, plugging Theorem 4 into Theorem 1, yields our theoretical results on an upper bound of $p^{\text{cov}}(\lambda, \gamma)$, which is particularly useful for sparse networks.

C. The Area Spectral Efficiency

We also investigate the area spectral efficiency (ASE) performance in bps/Hz/km², which is defined as [10]

$$A^{\text{ASE}}(\lambda, \gamma_0) = \tilde{\lambda} \int_{\gamma_0}^{+\infty} \log_2(1 + \gamma) f_{\Gamma}(\lambda, \gamma) d\gamma, \quad (26)$$

where γ_0 is the minimum working SINR in a practical SCN, and $f_{\Gamma}(\lambda, \gamma)$ is the PDF of the SINR γ observed at the typical UE for a particular value of λ . Based on the definition of $p^{\text{cov}}(\lambda, \gamma)$ in (19) and the partial integration theorem [14], (26) can be reformulated as

$$A^{\text{ASE}}(\lambda, \gamma_0) = \frac{\tilde{\lambda}}{\ln 2} \int_{\gamma_0}^{+\infty} \frac{p^{\text{cov}}(\lambda, \gamma)}{1 + \gamma} d\gamma + \tilde{\lambda} \log_2(1 + \gamma_0) p^{\text{cov}}(\lambda, \gamma_0). \quad (27)$$

IV. SIMULATION AND DISCUSSION

In this section, we investigate network performance and use numerical results to validate the accuracy of our analysis. According to Tables A.1-3, A.1-4 and A.1-7 of [15], we adopt the following parameters for the 3GPP Case: $\alpha^L = 2.09$, $\alpha^{\text{NL}} = 3.75$, $A^L = 10^{-10.38}$, $A^{\text{NL}} = 10^{-14.54}$, $P = 24$ dBm, $P_N = -95$ dBm (including a noise figure of 9 dB at each UE). Besides, the UE density ρ is set to 300 UEs/km², which leads to $q = 4.05$ in (1) and (2) [13].

A. The Coverage Probability Performance of the 3GPP Case

In Fig. 1, we plot the results of $p^{\text{cov}}(\lambda, \gamma)$ with the PF scheduler for the 3GPP Case when $\rho = 300$ UEs/km² and $\gamma = 0$ dB. Note that our analytical results on the exact performance are obtained from Theorems 1 and 2. In contrast, our analytical results on the upper-bound performance are obtained from Theorems 1 and 4. As a benchmark, we also provide simulation results, and display the analytical results of the RR scheduler reported in [13]. Moreover, we show the ratio of the simulated $p^{\text{cov}}(\lambda, \gamma)$ of the PF scheduler to that of the RR scheduler in Fig. 2.

From these two figures, we can observe that:

- As can be seen from Fig. 1, our analytical results well match the simulation results, which validates the accuracy of Theorems 1 and 2. However, as discussed in Subsection III-A, the evaluation of our analytical results is only efficient for dense and ultra-dense networks. Thus, in Fig. 1, we are only able to show the results of $p^{\text{cov}}(\lambda, \gamma)$ for $\lambda \geq 100$ BSs/km². When $\lambda < 100$ BSs/km², the proposed upper-bound results in Theorems 1 and 4 successfully capture the qualitative performance trend of the PF scheduler, with a maximum error of 0.04 in terms of $p^{\text{cov}}(\lambda, \gamma)$ for sparse networks.
- As predicted in Lemma 3, although the PF scheduler shows a better performance than the RR one for all BS densities, such performance gain diminishes as the network evolves into an UDN due to the loss of multi-user diversity. As can be seen from Fig. 2, the performance gain of the PF scheduler continuously decreases from around 175 % (ratio=2.75) when $\lambda = 1$ BSs/km² toward zero (ratio=1) in UDNs, e.g., $\lambda = 10^4$ BSs/km².

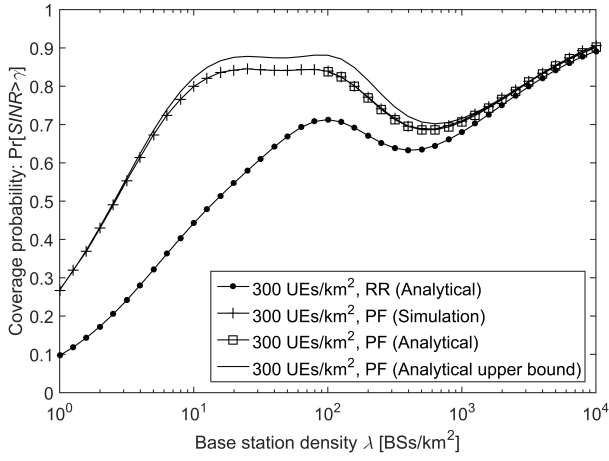


Fig. 1. The coverage probability $p^{\text{cov}}(\lambda, \gamma)$ vs. λ for the 3GPP Case with Rayleigh fading ($\rho = 300$ UEs/km², $\gamma = 0$ dB).

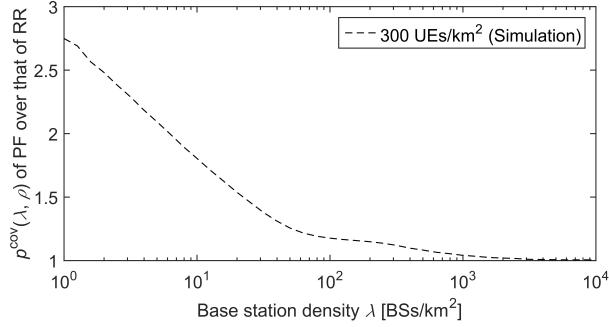


Fig. 2. The ratio of the simulated $p^{\text{cov}}(\lambda, \gamma)$ of PF to that of RR for the 3GPP Case with Rayleigh fading ($\rho = 300$ UEs/km², $\gamma = 0$ dB).

- The detailed explanation of the performance behavior in Fig. 1 is provided as follows:
 - When $\lambda \in [10^0, 10^1]$ BSs/km², the network is noise-limited, and thus the coverage probabilities of both RR and PF increase with the BS density λ as the network is lightened up with more BSs.
 - When $\lambda \in [10^1, 10^2]$ BSs/km², $p^{\text{cov}}(\lambda, \gamma)$ of the PF scheduler shows an interesting flat trail. This is because (i) the signal power is enhanced by LoS transmissions, as shown by the $p^{\text{cov}}(\lambda, \gamma)$ of the RR scheduler in that BS density region; while (ii) the multi-user diversity decreases in that BS density region as exhibited in Fig. 2; and (iii) the above two factors roughly cancel each other out.
 - When $\lambda \in [10^2, 10^3]$ BSs/km², the coverage probabilities of both RR and PF decrease with λ , as the network is pushed into the interference-limited region, and this performance degradation is due to the transition of a large number of interfering paths from NLoS to LoS, which accelerates the growth of the aggregate inter-cell interference [10].
 - When $\lambda > 10^3$ BSs/km², the coverage probabilities of both RR and PF continuously increase [13]. Such performance behavior can be attributed to the BS idle mode operations, i.e., (i) the signal power continues

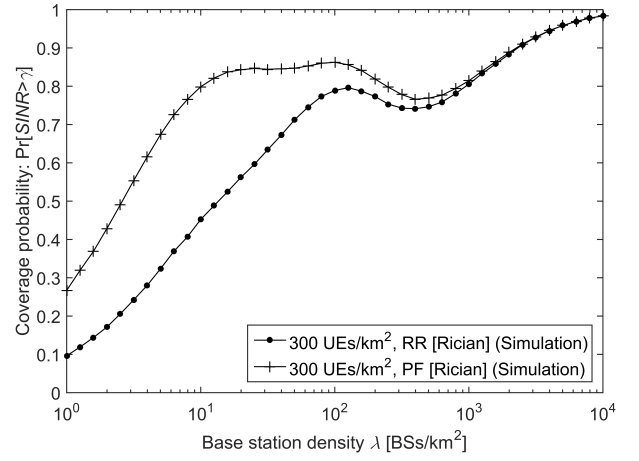


Fig. 3. The coverage probability $p^{\text{cov}}(\lambda, \gamma)$ vs. λ for the 3GPP Case with distance-dependent Rician fading ($\rho = 300$ UEs/km², $\gamma = 0$ dB).

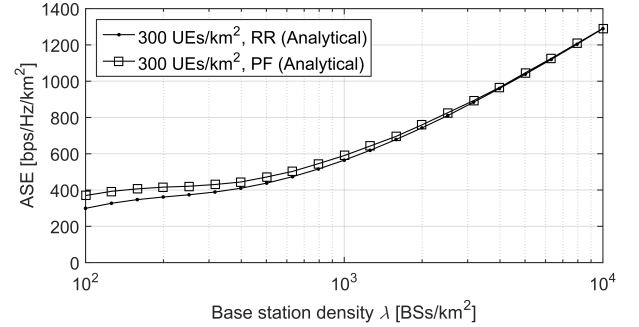


Fig. 4. The ASE $A^{\text{ASE}}(\lambda, \gamma_0)$ vs. λ for the 3GPP Case with Rayleigh fading ($\rho = 300$ UEs/km², $\gamma_0 = 0$ dB).

increasing with the network densification, and (ii) the interference power is controlled because not all BSs are turned on and emit interference.

B. The Performance Impact of Rician Fading

In this subsection, we investigate the performance for the 3GPP Case with **distance-dependent Rician fading**, which has been introduced in Subsection II-B. Due to its complex modeling, we conduct simulations to investigate this enhanced 3GPP Case, and the results are plotted in Fig. 3.

All the conclusions in Subsections IV-A are qualitatively valid for Fig. 3, which shows the usefulness of our analysis and a less urgency to consider Rician fading in this performance analysis. Note that comparing Fig. 3 with Fig. 1, we can see that Rician fading closes the performance gap between PF and RR more quickly than Rayleigh fading, due to its less variance in channel fluctuation for the PF scheduler to exploit.

C. The ASE Performance of the 3GPP Case

Finally, we investigate the ASE performance, which is calculated from the results of $p^{\text{cov}}(\lambda, \gamma)$ using (26). Since the analytical results of $p^{\text{cov}}(\lambda, \gamma)$ obtained from Theorems 1 and 2 have been validated in Fig. 1, we only plot the analytical results of $A^{\text{ASE}}(\lambda, \gamma_0)$ for the PF and RR schedulers in Fig. 4. Note that we only investigate dense and ultra-dense SCNs with

$\lambda \geq 100 \text{ BSs/km}^2$ in Fig. 4 because they are the focus of 5G and Theorem 2 is computationally efficient to evaluate them.

As can be seen from this figure, the ASE performance of the PF scheduler quickly converges to that of the RR scheduler in UDNs, e.g., when $\lambda = 10^3 \text{ BSs/km}^2$, the ASE of the PF scheduler is around 590.1 bps/Hz/km², which is merely 4.52 % higher than that of the RR scheduler around 564.6 bps/Hz/km². Such gain becomes practically zero as λ further increases.

V. CONCLUSION

In this paper, we studied the network performance of the PF scheduler. Analytical results that are computationally efficient have been derived for dense and ultra-dense SCNs. For sparse networks, easy-to-compute analytical results of an upper-bound performance have been obtained to achieve a balance between accuracy and efficiency. Considering the negligible gain of the more complex channel-dependent PF scheduling in UDNs, it is recommended to adopt simpler scheduling mechanisms such as the RR scheduler to simplify the RRM, and thus reduce network complexity for UDNs. As our future work, a non-full-buffer traffic model [18, 19] will be studied.

APPENDIX A: PROOF OF THEOREM 1

Due to the page limit, we only provide the proof sketch of Theorem 1 as follows. In (10), T_n^L and T_n^{NL} are the components of the coverage probability for the case when the signal comes from the n -th piece LoS path and for the case when the signal comes from the n -th piece NLoS path, respectively. The calculation of T_n^L is based on (11), in which $f_{R,n}^L(r)$ characterizes the geometrical density function of the typical UE with no other LoS BS and no NLoS BS providing a better link to the typical UE than its serving BS (a BS with the n -th piece LoS path). Besides, $\mathbb{E}_{[\tilde{k}]} \left\{ \Pr \left[\frac{P\zeta_n^L(r)y(\tilde{k})}{I_{\text{agg}} + P_N} > \gamma \right] \right\}$ gives the expected coverage probability over all possible values of \tilde{k} on condition of r . The logic of the calculation of T_n^{NL} is similar to that of T_n^L .

APPENDIX B: PROOF OF THEOREM 2

Due to the page limit, here we only provides the key of the proof for Theorem 2. The derivation of (13) is as follows,

$$\begin{aligned} & \mathbb{E}_{[\tilde{k}]} \left\{ \Pr \left[\frac{P\zeta_n^L(r)y(\tilde{k})}{I_{\text{agg}} + P_N} > \gamma \right] \right\} \\ &= \mathbb{E}_{[\tilde{k}]} \left\{ \Pr \left[y(\tilde{k}) > \frac{\gamma(I_{\text{agg}} + P_N)}{P\zeta_n^L(r)} \right] \right\} \\ &\stackrel{(a)}{=} \mathbb{E}_{[\tilde{k}, I_{\text{agg}}]} \left\{ \bar{F}_Y(\tilde{k}) \left(\frac{\gamma(I_{\text{agg}} + P_N)}{P\zeta_n^L(r)} \right) \right\} \\ &\stackrel{(b)}{=} \sum_{\tilde{k}=1}^{\tilde{K}^{\max}} \mathbb{E}_{[I_{\text{agg}}]} \left\{ 1 - \sum_{t=0}^{\tilde{k}} \binom{\tilde{k}}{t} (-\delta_n^L(r))^t \exp(-sI_{\text{agg}}) \right\} f_{\tilde{K}}(\tilde{k}), \end{aligned} \quad (28)$$

where the step (a) of (28) comes from (23), and in the step (b) of (28) $s = \frac{\gamma}{P\zeta_n^L(r)}$ and $\mathbb{E}_{[I_{\text{agg}}]} \{ \exp(-sI_{\text{agg}}) \} = \mathcal{L}_{I_{\text{agg}}}^L(s)$ should be further plugged into (28) to obtain (13). The calculation of $\mathcal{L}_{I_{\text{agg}}}^L(s)$ can be referred to [13]. The derivation of (16) is very similar to (28), which is omitted for brevity.

APPENDIX C: PROOF OF LEMMA 3

The key of the proof for Lemma 3 lies in (13) and (16) of Theorem 2. When $\lambda \rightarrow +\infty$, we have that $\tilde{K}^{\max} \rightarrow 1$ and $f_{\tilde{K}}(1) = 1$. Hence, Theorem 2 will degenerate to the results for the RR scheduler addressed in [13].

APPENDIX D: PROOF OF THEOREM 4

The key of the proof for Theorem 4 lies in using Jensen's inequality as follows [14]

$$\mathbb{E}_{[I_{\text{agg}}]} \left\{ 1 - (1 - \exp(-x))^{\tilde{k}} \right\} \leq 1 - (1 - \mathbb{E}_{[I_{\text{agg}}]} \{ \exp(-x) \})^{\tilde{k}}. \quad (29)$$

REFERENCES

- [1] D. López-Pérez, M. Ding, H. Claussen, and A. Jafari, "Towards 1 Gbps/UE in cellular systems: Understanding ultra-dense small cell deployments," *IEEE Communications Surveys Tutorials*, vol. 17, no. 4, pp. 2078–2101, Jun. 2015.
- [2] 3GPP, "TR 36.872: Small cell enhancements for E-UTRA and E-UTRAN - Physical layer aspects," Dec. 2013.
- [3] X. Ge, S. Tu, G. Mao, C. X. Wang, and T. Han, "5G ultra-dense cellular networks," *IEEE Wireless Communications*, vol. 23, no. 1, pp. 72–79, Feb. 2016.
- [4] J. G. Choi and S. Bahk, "Cell-throughput analysis of the proportional fair scheduler in the single-cell environment," *IEEE Transactions on Vehicular Technology*, vol. 56, no. 2, pp. 766–778, Mar. 2007.
- [5] E. Liu and K. K. Leung, "Expected throughput of the proportional fair scheduling over rayleigh fading channels," *IEEE Communications Letters*, vol. 14, no. 6, pp. 515–517, Jun. 2010.
- [6] J. Wu, N. B. Mehta, A. F. Molisch, and J. Zhang, "Unified spectral efficiency analysis of cellular systems with channel-aware schedulers," *IEEE Transactions on Communications*, vol. 59, no. 12, pp. 3463–3474, Dec. 2011.
- [7] F. Liu, J. Riihijärvi, and M. Petrova, "Robust data rate estimation with stochastic sinr modeling in multi-interference ofdma networks," *2015 12th Annual IEEE International Conference on Sensing, Communication, and Networking (SECON)*, pp. 211–219, Jun. 2015.
- [8] A. H. Jafari, D. López-Pérez, M. Ding, and J. Zhang, "Study on scheduling techniques for ultra dense small cell networks," *Vehicular Technology Conference (VTC Fall), 2015 IEEE 82nd*, pp. 1–6, Sep. 2015.
- [9] M. Haenggi, *Stochastic Geometry for Wireless Networks*. Cambridge University Press, 2012.
- [10] M. Ding, P. Wang, D. López-Pérez, G. Mao, and Z. Lin, "Performance impact of LoS and NLoS transmissions in dense cellular networks," *IEEE Transactions on Wireless Communications*, vol. 15, no. 3, pp. 2365–2380, Mar. 2016.
- [11] M. Ding, D. López-Pérez, and G. Mao, "A new capacity scaling law in ultra-dense networks," *arXiv:1704.00399 [cs.NI]*, Apr. 2017. [Online]. Available: <https://arxiv.org/abs/1704.00399>
- [12] S. Lee and K. Huang, "Coverage and economy of cellular networks with many base stations," *IEEE Communications Letters*, vol. 16, no. 7, pp. 1038–1040, Jul. 2012.
- [13] M. Ding, D. López-Pérez, G. Mao, and Z. Lin, "Study on the idle mode capability with LoS and NLoS transmissions," *IEEE Globecom 2016*, pp. 1–6, Dec. 2016.
- [14] I. Gradshteyn and I. Ryzhik, *Table of Integrals, Series, and Products (7th Ed.)*. Academic Press, 2007.
- [15] 3GPP, "TR 36.828: Further enhancements to LTE Time Division Duplex for Downlink-Uplink interference management and traffic adaptation," Jun. 2012.
- [16] Spatial Channel Model AHG, "Subsection 3.5.3, Spatial Channel Model Text Description V6.0," Apr. 2003.
- [17] H. A. David and H. N. Nagaraja, *Order Statistics (3rd Edition)*. John Wiley & Sons, Inc., 2003.
- [18] M. Ding, D. López-Pérez, R. Xue, A. Vasilakos, and W. Chen, "On dynamic Time-Division-Duplex transmissions for small-cell networks," *IEEE Transactions on Vehicular Technology*, vol. 65, no. 11, pp. 8933–8951, Nov. 2016.
- [19] Y. Zhong, T. Q. S. Quek, and X. Ge, "Heterogeneous cellular networks with spatio-temporal traffic: Delay analysis and scheduling," *IEEE Journal on Selected Areas in Communications*, vol. 35, no. 6, pp. 1373–1386, Jun. 2017.